OPEN ACCESS

University of Dundee

University of Dundee

A stable phantom material for optical and acoustic imaging

Hacker, Lina; Ivory, Aoife M.; Joseph, James; Gröhl, Janek; Zeqiri, Bajram; Rajagopal, Srinath

Published in:
JoVE: Journal of Visualized Experiments

DOI:
10.3791/65475

Publication date:
2023

Licence:
CC BY

Document Version
Publisher's PDF, also known as Version of record

Link to publication in Discovery Research Portal

Citation for published version (APA):
Hacker, L., Ivory, A. M., Joseph, J., Gröhl, J., Zeqiri, B., Rajagopal, S., & Bohndiek, S. E. (2023). A stable phantom material for optical and acoustic imaging. *JoVE: Journal of Visualized Experiments*, *196*, [e65475]. https://doi.org/10.3791/65475

General rights
Copyright and moral rights for the publications made accessible in Discovery Research Portal are retained by the authors and/or other copyright owners and it is a condition of accessing publications that users recognise and abide by the legal requirements associated with these rights.

• Users may download and print one copy of any publication from Discovery Research Portal for the purpose of private study or research.
• You may not further distribute the material or use it for any profit-making activity or commercial gain.
• You may freely distribute the URL identifying the publication in the public portal.

Take down policy
If you believe that this document breaches copyright please contact us providing details, and we will remove access to the work immediately and investigate your claim.

Download date: 31. Jul. 2023

A Stable Phantom Material for Optical and Acoustic Imaging

Lina Hacker[1,2], **Aoife M. Ivory**[3], **James Joseph**[4,5], **Janek Gröhl**[1,2], **Bajram Zeqiri**[3], **Srinath Rajagopal**[3], **Sarah E. Bohndiek**[1,2]

[1] Department of Physics, University of Cambridge [2] Cancer Research UK Cambridge Institute, University of Cambridge [3] Ultrasound and Underwater Acoustics Group, Department of Medical, Marine and Nuclear Physics, National Physical Laboratory [4] School of Science and Engineering, University of Dundee [5] Centre for Medical Engineering and Technology, University of Dundee

Corresponding Author

Sarah E. Bohndiek
seb53@cam.ac.uk

Citation

Hacker, L., Ivory, A.M., Joseph, J., Gröhl, J., Zeqiri, B., Rajagopal, S., Bohndiek, S.E. A Stable Phantom Material for Optical and Acoustic Imaging. *J. Vis. Exp.* (196), e65475, doi:10.3791/65475 (2023).

Date Published

June 16, 2023

DOI

10.3791/65475

URL

jove.com/video/65475

Abstract

Establishing tissue-mimicking biophotonic phantom materials that provide long-term stability are imperative to enable the comparison of biomedical imaging devices across vendors and institutions, support the development of internationally recognized standards, and assist the clinical translation of novel technologies. Here, a manufacturing process is presented that results in a stable, low-cost, tissue-mimicking copolymer-in-oil material for use in photoacoustic, optical, and ultrasound standardization efforts.

The base material consists of mineral oil and a copolymer with defined Chemical Abstract Service (CAS) numbers. The protocol presented here yields a representative material with a speed of sound c(f) = 1,481 ± 0.4 $m \cdot s^{-1}$ at 5 MHz (corresponds to the speed of sound of water at 20 °C), acoustic attenuation α(f) = 6.1 ± 0.06 $dB \cdot cm^{-1}$ at 5 MHz, optical absorption $\mu_a(\lambda)$ = 0.05 ± 0.005 mm^{-1} at 800 nm, and optical scattering $\mu_s'(\lambda)$ = 1 ± 0.1 mm^{-1} at 800 nm. The material allows independent tuning of the acoustic and optical properties by respectively varying the polymer concentration or light scattering (titanium dioxide) and absorbing agents (oil-soluble dye). The fabrication of different phantom designs is displayed and the homogeneity of the resulting test objects is confirmed using photoacoustic imaging.

Due to its facile, repeatable fabrication process and durability, as well as its biologically relevant properties, the material recipe has high promise in multimodal acoustic-optical standardization initiatives.

Introduction

Establishing the precision and accuracy of novel optical imaging biomarkers through technical validation[1,2] is paramount to ensuring their successful implementation in clinical practice. To achieve this, technical validation studies

Copyright © 2023 JoVE Creative Commons Attribution 3.0 License

frequently employ durable physical phantoms, which facilitate inter-instrument performance assessment and routine quality control. For widespread use of a phantom material in research and clinical translation, a simple, highly reproducible fabrication protocol is required. An ideal biophotonic phantom material should include the following properties[3]: (1) independently tunable properties within biologically relevant ranges; (2) mechanical robustness; (3) long-term stability; (4) flexibility in geometry and architecture; (5) safe handling; (6) widely available ingredients that can be purchased from standard scientific suppliers; and (7) low cost. At present, biophotonic applications lack a standardized protocol for a widely accepted phantom material that fulfils the outlined requirements and also includes tunable acoustic properties for hybrid applications, such as photoacoustic imaging (PAI).

Biologically relevant phantom materials targeted for combined optical and acoustic applications include hydrogels[4,5], polyvinyl alcohol (PVA)[6,7,8,9], and polyvinyl chloride plastisol (PVCP)[10,11,12,13,14,15,16]. However, these materials are characterized by certain limitations that restrict their application as a stable phantom material. Hydrogels, for example, are prone to dehydration, mechanical damage, and bacterial ingrowth, limiting their shelf life[17,18,19]. The addition of chemicals can increase the longevity, but common preservatives, such as formaldehyde[20] or benzalkonium chloride[21], are hazardous and require cautionary measures during handling. Additionally, targets containing water-soluble dyes can diffuse within the base material if not encapsulated. PVA cryogels are characterized by a higher longevity and structural robustness, but their preparation process involves long freeze-thaw cycles[22]. This can limit the independent tunability of acoustic and optical parameters[23] and-if slightly varied-can lead to inhomogeneities[6], thereby compromising reproducibility. Moreover, the diffusion of dyes from inclusions has been observed after 1 year[13]. PVCP has a complex fabrication process that includes high temperatures of up to 180-220 °C[13,14,24,25]. PVCP also suffers from a lack of a supply chain with scientific suppliers[26] and can contain plasticizers based on phthalates, which may cause reproductive and developmental harm[27], making them controlled substances in some countries.

Copolymer-in-oil compositions, such as gel wax[28,29,30,31] or blends based on thermoplastic styrenic elastomers[32,33,34,35,36], exhibit good longitudinal stability and feature tissue-like acoustic and optical properties[31,35,36,37], thereby having high potential as a durable phantom candidate in multimodal applications. Additionally, this class of material is cost-effective, non-water absorbing, non-toxic, and biologically inert[35,38]. The speed of sound c(f) and acoustic attenuation coefficient α(f) can be tuned in a biologically relevant range (**Table 1**) by variation of the polymer concentration[33,35,39], whilst optical absorption $\mu_a(\lambda)$ and reduced scattering $\mu_s'(\lambda)$ coefficients can be primarily varied by the addition of oil-soluble dyes or titanium dioxide (TiO_2)[39], respectively.

Here, a simple, easy-to-follow protocol is presented for the creation of durable copolymer-in-oil phantoms suitable for use in optical, ultrasound, or photoacoustic device calibration. All ingredients have defined Chemical Abstract Service (CAS) numbers and are readily available from standard scientific suppliers. Potential difficulties in the fabrication procedure are highlighted and ways to overcome them are presented. Whilst the protocol allows the fabrication of materials with a range of acoustic and optical properties, the presented protocol yields a material with a speed of sound of ~1,481 $m \cdot s^{-1}$, aligning with the speed of sound of water at room temperature (20 °C)[40].

Copyright © 2023 JoVE Creative Commons Attribution 3.0 License

This value was selected as a neutral standard for representing the wide range of existing tissue properties (**Table 1**), allowing the establishment of a consistent and reliable reference point for comparison. By providing this detailed protocol, we aim to broaden the uptake and manufacturing reproducibility of this promising phantom material type, thereby facilitating biophotonic, acoustic, and photoacoustic validation studies and supporting routine quality control in preclinical and clinical imaging applications.

Protocol

Table 1: Overview of acoustic and optical properties found in soft tissues. Optical properties cover a spectrum ranging from 600 to 900 nm. It should be noted that these are only representative values intended to provide general guidance. Precise values may vary depending on the experimental condition (e.g., temperature) and frequency/ wavelength. The literature provides more specific values. *No specific reference found. Please click here to download this Table.

The given protocol has been developed for making ~120 mL of phantom material. The masses of the components can be scaled to make different volumes of phantom material. Please note that for larger volumes (>500 mL), the proposed equipment may not be able to sufficiently heat the phantom mixture homogenously. For this purpose, heating equipment should be adapted appropriately.

CAUTION: Always ensure suitable personal protective equipment (PPE) is worn throughout the entire fabrication process. This may include the use of lab coats, safety goggles, and safety gloves; refer and adhere to local safety guidelines. The procedure is adapted from Hacker et al.[39]; a summary of the steps is displayed in **Figure 1**.

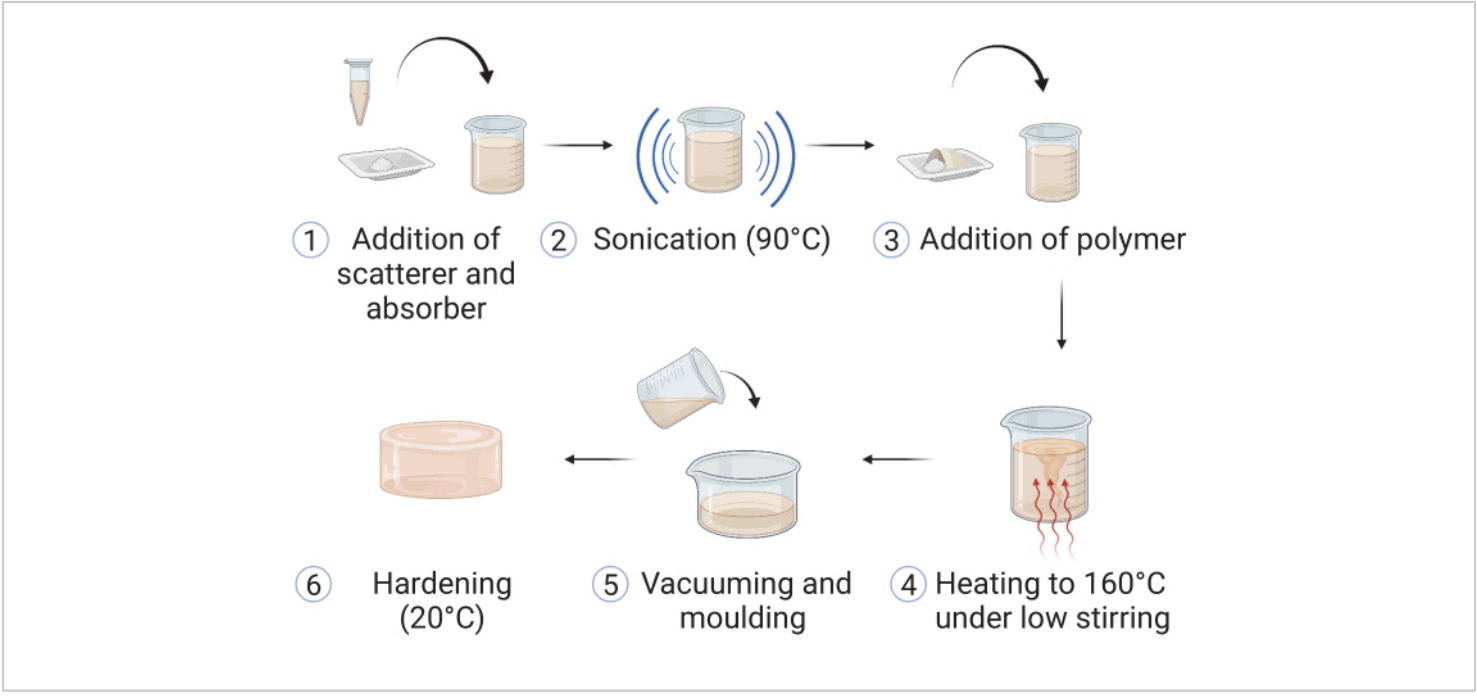

Figure 1: Fabrication of the copolymer-in-oil material. (1) Materials for optical scattering and absorption are added to mineral oil and (2) sonicated at 90 °C until dissolved. (3) Polymer(s) and stabilizer are added, and (4) the mixture is heated

Copyright © 2023 JoVE Creative Commons Attribution 3.0 License

up in an oil bath to 160 °C under low stirring. (5) Upon dissolution of all the components, the sample is poured into a suitable phantom mold and (6) left to harden at room temperature. This figure is reproduced from Hacker et al.[39]. Please click here to view a larger version of this figure.

1. Preparation of the mixture

1. Prepare the Nigrosin stock solution by adding 0.4 g of Nigrosin to 40 mL of mineral oil. Ensure homogeneous mixing by sonication and thorough vortexing of the sample. Store the stock solution at room temperature.
   NOTE: The stock solution should always be thoroughly mixed before reuse. If a phantom material without an optical scatterer (TiO_2) or absorber (dye) is preferred, step 1 and 2 can be skipped. Proceed with step 3.
2. Sonicate 0.15 g of TiO_2 and 1 mL of the dye stock solution in 100 mL (83.8 g) of mineral oil until all the components have been completely dissolved (~60 min) (**Figure 1**: steps 1 and 2). Set the sonicator to elevated temperatures (90 °C) if the equipment allows, as this facilitates the mixing process. Proceed with steps 3-5 during the sonication time.
   NOTE: If a phantom with higher absorbing and scattering properties is preferred, the sonication time may need to be extended.
3. Weigh out the polystyrene-block-poly(ethylene-ran-butylene)-block-polystyrene (SEBS) and low-density polyethylene (LDPE) at the desired concentrations (e.g., SEBS = 25.14 g; LDPE = 6.70 g) (**Figure 1**: step 3).
   1. Optional: An antioxidant may be added to increase stability, but it is not obligatory if the heating temperatures do not exceed 180°C.
      NOTE: In case solubility or viscosity issues are encountered at a later stage of the manufacturing process, it is advisable to exclude the LDPE. LDPE is incorporated to enhance the speed of sound in the material (**Table 3**); however, it is not mandatory for creating a stable phantom. By omitting LDPE, the manufacturing and molding process can be simplified, but it will result in a decrease in the subsequent speed of sound of the final material (**Table 3**).
4. Create an oil bath using suitable glassware and silicone oil; carefully secure it on the hotplate. Ensure the thermocouple remains in the silicone oil bath and does not touch the edges of the glassware throughout the procedure (**Figure 2**).
   NOTE: Ensure that the thermoregulatory accessory is carefully mounted, as instructed by the equipment manufacturer.
5. Place a magnetic stir bar of adequate length inside the oil bath to ensure uniform heat distribution.
6. Turn on the hotplate, set the heating temperature to 160 °C, and set the revolutions per minute (rpm) of the stirrer to 50.
7. Transfer the LDPE and SEBS into the glass beaker containing the sonicated mineral oil (with TiO_2 and Nigrosin). Introduce a magnetic stir bar of adequate length into the glass beaker and transfer it into the center of the oil bath for heating of the measured components. Ensure that the oil level in the bath remains above the mineral oil level inside the beaker (**Figure 1**: step 4).

Copyright © 2023 JoVE Creative Commons Attribution 3.0 License

2. Heating the mixture

1. If at any stage the added polymer appears to float over the mineral oil, manually stir the mineral oil solution using a metallic spatula, so that any floating polymer is distributed inside the mineral oil. Wear heat-resistant gloves.
2. Leave the mixture at 160 °C until all the polymer has dissolved and the solution appears uniformly mixed, with a smooth and homogeneous texture (~1.5 h).

3. Vacuuming

NOTE: For removal of air bubbles, follow the following steps, depending on the equipment available.

1. Place the hot beaker carefully into the **vacuum chamber** and vacuum the samples for 2-3 min on the highest setting (lowest vacuum). Use a metallic spatula to carefully remove any air bubbles that accumulate on the surface. If air bubbles are still present after this step, reheat the mixture and repeat the vacuuming step until all air bubbles have been removed.
2. Turn on the **vacuum oven** and heat it up to 160 °C. Once it has reached the desired temperature, transfer the beaker with the solution into the vacuum oven.
   NOTE: Always handle the beaker with heat protective gloves.
   1. Switch on the vacuum to the highest setting (lowest vacuum) available. If a foam layer has produced on top of the solution, turn off the vacuum and remove the bubbles from the surface using a spatula (repeat this step until all air bubbles have been removed).
   2. Leave the beaker in the vacuum oven for 1 h at the highest vacuum setting.

   NOTE: To keep the vacuum oven clean, clean the external surface of the beaker of silicone oil with a paper towel.

4. Pouring the samples into the mold

1. Before pouring the samples into sample molds, remove any remaining air bubbles on the surface of the mixture with a spatula if necessary.
2. Carefully pour the solution into a suitable mold, wearing heat-resistant gloves or using adequate protective equipment. Ensure smooth and steady pouring from a low height to reduce the chance of any air bubbles forming (**Figure 1**: step 5). For molds with complex shapes, coat the mold with a thin layer of oil (other than mineral oil [e.g., castor or silicone oil]) prior to pouring to facilitate removal of the cured sample.
   NOTE: Preheating of the molds in an oven can help with achieving higher sample homogeneity.
3. Remove any air bubbles from the top of the samples quickly with a metallic spatula once poured. If numerous air bubbles have accumulated within the mixture, repeat the vacuum step, provided that the type and shape of the mold permits it.
4. Allow the solution to set at room temperature. Although smaller samples may cure in less than 2 h, leave the samples overnight to eliminate any risk of incomplete curing. Store the samples at room temperature (**Figure 1**: step 6).

5. Image acquisition

1. For image acquisition, place the phantom in the field of view of the imaging device.

Copyright © 2023 JoVE Creative Commons Attribution 3.0 License

2. For PAI or ultrasound systems, perform acoustic coupling of the phantom surface to the ultrasound transducer, for example, with ultrasound gel or water.

   NOTE: If the protocol has been followed correctly, no inhomogeneities should perturb the field of view. Custom phantom holders can assist in repeatable sample positioning between measurements.

3. If the acquisition temperature differs from the storing temperature of the phantom, allow the phantom temperature to stabilize with the surroundings.

4. Acquire an image.

6. Material characterization measurements

NOTE: The purpose of material characterization measurements is verification of the material optical and acoustic properties. It should be noted that the phantom fabrication protocol has shown high reproducibility[39], so the general measurement protocols that follow are only provided as guidance if further verification studies are desired. The individual steps of the measurements will depend on the characterization equipment used. Here, a system based on a broadband through-transmission substitution method[41] (available at the National Physical Laboratory (NPL), UK) was employed for acoustic characterization and an in-house double-integrating-sphere (DIS) system was used (based on [42]) for optical characterization. The setup of the characterization systems is displayed in **Supplementary Figure 1**. Additional details on the measurement setups (acoustic[43]; optical[42,44]) and measurement procedure[39] can be found elsewhere. The measurement procedure should be adapted accordingly to each specific characterization system used.

1. Acoustic characterization

   NOTE: The acoustic characterization measurements are based on a system employing a 10 MHz center frequency ultrasound transducer (active element diameter of 10 mm) for pulse generation and a broadband hydrophone (30 mm active element diameter bilaminar membrane hydrophone) for pulse detection (both placed in a water tank filled with deionized water; dimensions of 112 cm x 38 cm x 30 cm^3). The transducer is driven by a pulser-receiver. Waveforms are acquired using an oscilloscope. More details on the setup and measurement procedure (including system-specific type B effects on the measurements) can be found in [43].

   1. Prepare samples suitable for the measurement setup (e.g., in this case, circular samples with a diameter of 7-8 cm and thickness of 6-9 mm). Ensure that the samples are of homogeneous composition and free of any impurities, air bubbles, or surface irregularities.

   2. Measure the thickness of the test sample using vernier calipers and record the temperature of the water tank using a calibrated thermometer.

   3. Place the sample into the system. Ensure that the sample is correctly aligned with the components of the system.

      NOTE: An automatically controlled sample holder based on a gimbal mount[43] may assist in precise control of the rotation and tilt of the sample.

   4. Acquire four acoustic pulses for each measurement set: a reference through-water pulse with no sample present in the acoustic path; a through-sample transmission; and acoustic reflections received at the transmitter from the front and rear surfaces of the sample.

Copyright © 2023 JoVE Creative Commons Attribution 3.0 License

5. Derive the acoustic properties of the sample from the measurements. Calculate the speed of sound *c(f)* (in $m \cdot s^{-1}$) using the equation (**1**)[43].

$$c(f) = c_w \left[1 + 2 * \frac{\theta_w(f) - \theta_s(f)}{\theta_2(f) - \theta_1(f)}\right] \quad (1)$$

c_w depicts the temperature-dependent speed of sound of water, and $\theta_1(f)$, $\theta_2(f)$, $\theta_w(f)$, and $\theta_s(f)$ are the corresponding unwrapped phase spectra of the front-reflected, back-reflected, through-water, and through-sample voltage pulses, respectively. The frequency-dependent attenuation coefficient ($\alpha_i(f)$) of the material can be derived using the two-sample substitution technique shown in equation (**2**)[43].

$$\alpha_i(f) = -\frac{20}{d_2 - d_1}\left(\log_{10}\left[\frac{U_{s2}(f)}{U_{w2}(f)}\right] - \log_{10}\left[\frac{U_{s1}(f)}{U_{w1}(f)}\right]\right) + \alpha_w(f) \quad (2)$$

$U_w(f)$ and $U_s(f)$ are the respective voltage magnitude spectra of the through-water and through-sample pulse, $\alpha_w(f)$ is the attenuation coefficient of ultrasound (in $dB \cdot cm^{-1}$) of pure water at the specific water tank temperature[45], and d_1 and d_2 ($d_2 > d_1$) are two sample thicknesses.

NOTE: For the present protocol, the attenuation accounting for interfacial losses was assessed, finding its impact to be negligible.

6. Repeat the measurement more than three times at different positions on the test sample. Calculate the mean and standard deviation of the measurements to derive a final sample value.

2. Optical characterization

NOTE: For optical testing, a double-integrating sphere system was used (based on [42]), employing two integrating spheres (50 mm internal diameter) that are connected to two spectrometers *via* two optical fibers. The reflectance sphere is connected to a light source *via* a third optical fiber.

1. Prepare samples suitable for the measurement setup (e.g., in this case, rectangular samples with a width of 5.9 cm, height of 1.8 cm, and thickness ranging between 2 and 3 mm). Ensure that the samples are of homogeneous composition and free of any impurities, air bubbles, or surface irregularities.
2. Turn on the light source and allow it to stabilize according to the manufacturer's instructions (e.g., 15 min).
3. Determine the thickness of the sample using vernier calipers. If applicable, specify the wavelength range and step size for the measurement (e.g., 450-900 nm with a 1 nm step size).
4. Record the reference measurements for the transmission and reflectance sphere.
    1. For the reflectance sphere, first take an open port measurement by recording the reflectance value *R*0 with the transmittance sphere removed and light source turned on. Then, record the reflectance value *R*1 with a reference standard held in front of the reflectance sphere (light source turned on).
    2. For the transmittance sphere, first take a blocked beam measurement by recording the transmittance value *T*0 with the aligned reflectance and transmittance spheres and light source turned off. Then, take an incident beam measurement by recording the transmittance value *T*1 with the aligned reflectance and

Copyright © 2023 JoVE Creative Commons Attribution 3.0 License

transmittance spheres and light source turned on.

NOTE: A clean surface of the spheres and reference standard must be ensured for the measurements, as the adherence of dust or other contaminants may impact the performance of the components[46].

5. Place the sample between the spheres. Measure the reflectance *Rs* and transmittance *Ts* values. Ensure that the sample is not compressed, as this may impact the measurement accuracy. Placing one sphere on a motorized stage may help to accurately control the distance between the spheres by adapting it to the measured sample thickness.

6. Calculate the normalized reflectance M_R and transmittance M_T values using equations (**3**) and (**4**)[42].

$$M_R = r_{std} \cdot \frac{R_s - R_0}{R_1 - R_0} \quad (3)$$

$$M_T = \frac{T_s - T_0}{T_1 - T_0} \quad (4)$$

r_{std} depicts the intensity reflected from the 99% reflectance standard.

7. Enter the measured values into an inverse adding doubling (IAD) program (source code: http://omlc.org/software/iad/)[44] to estimate the optical properties of the material.

NOTE: Based on previous reports, the scattering anisotropy factor (g) can be taken as g = 0.7, and the refractive index as n = 1.4 [30].

8. Repeat the measurement at least three times at different positions along the test sample. Calculate the mean and standard deviation of the measurements to derive a final sample value.

Representative Results

Following this recipe, three representative phantom designs have been created for the purpose of photoacoustic imaging, targeted for different system designs with different optical illumination and acoustic detection geometries (**Figure 3A**). If the phantom preparation procedure is performed successfully, the phantom material appears smooth and homogeneous without any trapped air bubbles or impurities, and no artifacts can be seen in the resulting image (here visualized using photoacoustic imaging; **Figure 3B,C**). The protocol yields a representative material with a speed of sound c(f) = 1481 ± 0.4 $m \cdot s^{-1}$ (corresponding to the speed of sound of water at 20 °C[40]), acoustic attenuation α(f) = 6.1 ± 0.06 $dB \cdot cm^{-1}$ (both at 5 MHz), optical absorption $\mu_a(\lambda)$ = 0.05 ± 0.005 mm^{-1}, and optical scattering $\mu_s'(\lambda)$ = 1 ± 0.1 mm^{-1} (both at 800 nm) (uncertainty depicts the standard deviation from n = 3 independently produced batches by different operators; all measurements were carried out at room temperature [20 °C]).

The optical scattering coefficient can be tuned by the variation of TiO_2, whilst the optical absorption coefficient can be tuned by the addition of any oil-soluble dye, here demonstrated with Nigrosin (**Table 2** and **Figure 3D**). Whilst the values in **Table 2** are focused on lower absorbing and scattering tissues, such as muscle or breast (**Table 1**), we have not encountered any difficulties with adding absorbers and scatterers at higher concentrations. However, the addition of optical scatterers/absorbers at higher concentrations may require longer sonication times to achieve homogenous mixing of the solution.

Copyright © 2023 JoVE Creative Commons Attribution 3.0 License

The acoustic attenuation and speed of sound can be tuned by variation of the polymer concentration (**Table 3**). Here, tuning is thus far limited to a speed of sound range of ~1,450-1,516 $m \cdot s^{-1}$. Lower respective polymer concentrations may result in low physical stability of the sample, leading to plastic deformation over time[34]. Higher polymer concentrations result in brittleness and an uneven texture of the material. The range of acoustic properties may help to mimic tissues such as breast or fat (c = 1,450-1,480 $m \cdot s^{-1}$), but may be insufficient for tissues such as muscle or kidney (c > 1,520 $m \cdot s^{-1}$; **Table 1**).

Common error sources in phantom preparation include insufficient removal of air bubbles and inhomogeneous mixing of the base components (**Figure 4**). This can be minimized by vacuuming and careful pouring, and stirring/vortexing, respectively.

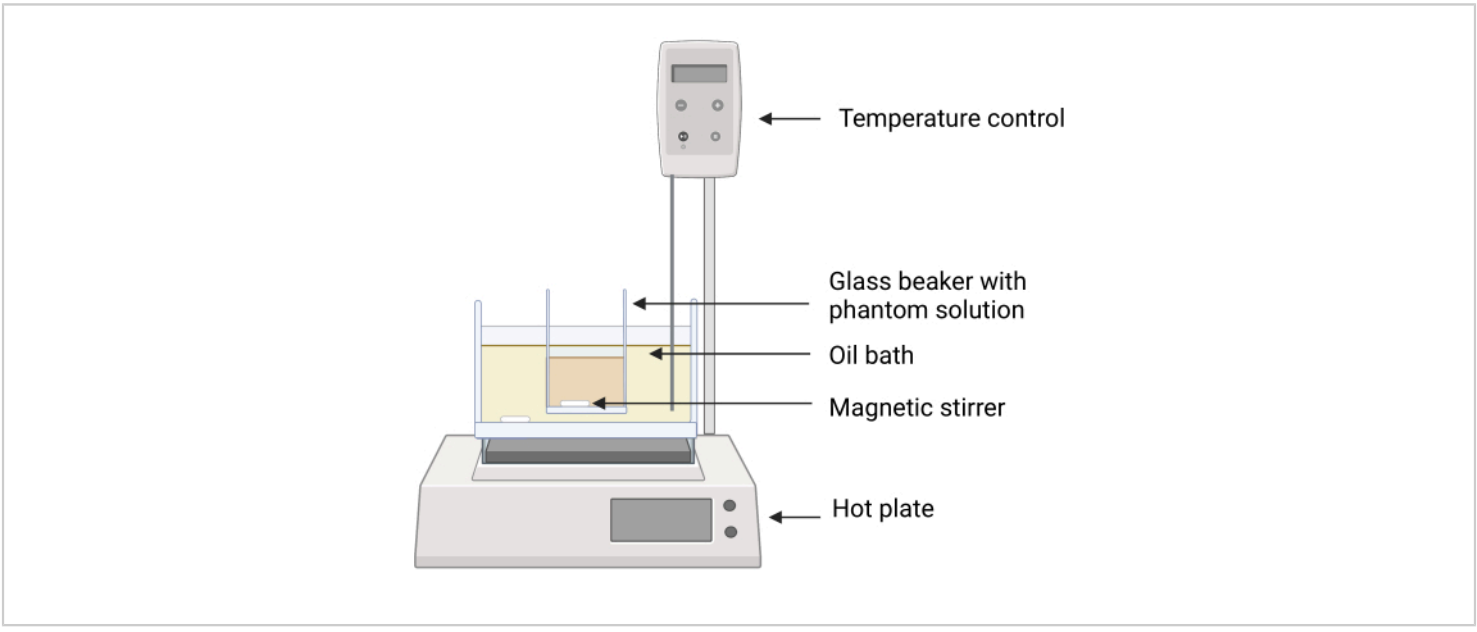

Figure 2: Experimental setup for the phantom fabrication. The glass beaker containing the phantom ingredients is placed in the silicone oil bath using a clamp to avoid direct contact between the surfaces of the oil bath and the glass beaker. Temperature feedback on the hot plate ensures careful temperature control. Magnetic stirrers enable mixing of the both the silicone oil and phantom ingredients. Please click here to view a larger version of this figure.

Copyright © 2023 JoVE Creative Commons Attribution 3.0 License

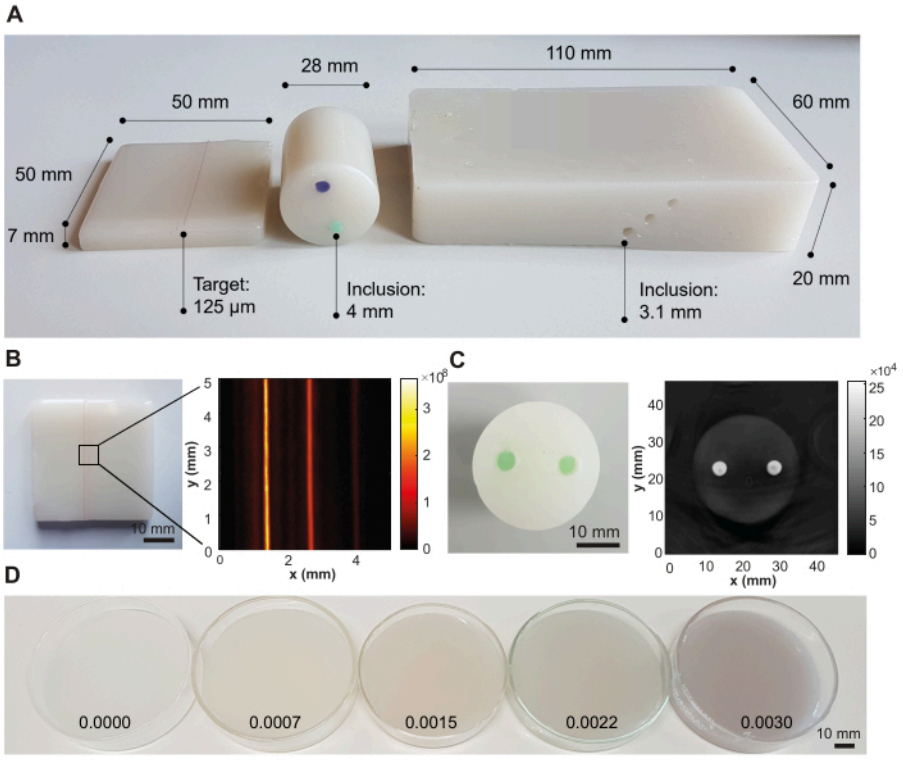

Figure 3: Representative results from the phantom fabrication procedure. (**A**) Various phantom designs showing versatility for application in different photoacoustic imaging systems. Left: small rectangular phantom with strings embedded at different depths (0.5, 1.5, and 2.5 mm; inter-target distance of 1.25 mm) designed for testing high-resolution imaging systems; middle: cylindrical phantom with two inclusions (inter-inclusion distance of 12 mm) using a green and violet oil-soluble dye, designed for testing tomography systems; right: large rectangular phantom with channels embedded at different depths (6 mm, 10 mm, and 14 mm; inter-inclusion distance of 3.5 mm), designed for testing a handheld system. (**B**) Example photoacoustic image of the rectangular phantom with embedded strings, acquired at 532 nm with a commercial photoacoustic imaging system. (**C**) Example photoacoustic image of the cylindrical tomographic phantom, acquired at 800 nm with a commercial photoacoustic imaging system. (**D**) Phantoms with increasing optical absorption concentrations by increasing concentrations of Nigrosin (concentrations given in weight percentage of the total volume of mineral oil on the image). **Figure 3B,C** is reproduced from Hacker et al.[39]. Scale bars = 10 mm. Please click here to view a larger version of this figure.

Copyright © 2023 JoVE Creative Commons Attribution 3.0 License

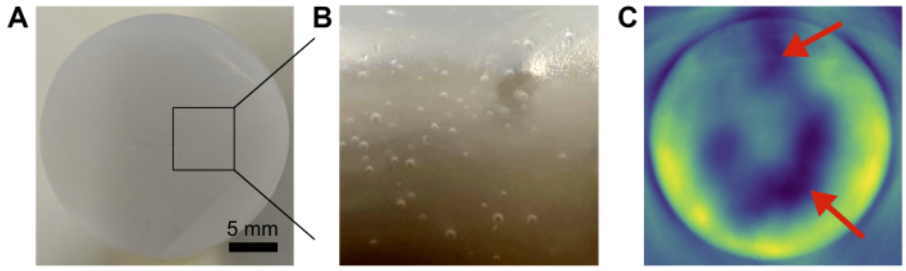

Figure 4: Common phantom failures. (**A**,**B**) Photographs showing air bubbles trapped inside the base matrix. (**C**) Insufficient mixing of base components leads to inhomogeneities (red arrows) in the resulting photoacoustic image. Scale bar = 5 mm (**A**). Please click here to view a larger version of this figure.

Table 2: Tabular overview of tuning of optical absorption (μ_a) and scattering (μ_s') values. Percentage values are given as weight percentage to the total volume of the base solution (mineral oil, column 1) and to the total weight of the phantom material (column 2). The Nigrosin concentrations depict the total amount of absolute Nigrosin (not stock solution). All samples included 5% butylated hydroxytoluene as an antioxidant (optional). n = 3 measurements per sample. A visual representation of the table can be found in Hacker et al.[39]. Abbreviation: neg = negligible. Please click here to download this Table.

Table 3: Tabular overview of tuning of acoustic attenuation (α) and speed of sound (c) values. Described by the power law $\alpha_0 f^n$ with α_0 and n parameters obtained from a non-linear least squares fitting (n = 4 measurements per sample). F depicts the frequency in MHz. Percentage values are given as weight percentage to the total weight of the base solution (mineral oil). All samples included 5% butylated hydroxytoluene as an antioxidant (optional). A visual representation of the table can be found in Hacker et al.[39]. Please click here to download this Table.

Supplementary Figure S1: Setup of the acoustic and optical characterization systems used for verifications. A photograph (**A**) and schematic (**B**) of the acoustic characterization system for determination of the acoustic attenuation coefficient and speed of sound are displayed. Individual system components are denoted by annotations HP (HydroPhone), S (Sample), and T (Transducer) in the photo and schematic. A photograph (**C**) and schematic (**D**) of the double-integrating sphere system for the evaluation of the optical absorption coefficient and reduced scattering coefficient are shown. Individual system components are denoted by annotations S (Sample), RS (Reflectance Sphere), TS (Transmission Sphere), OF (Optical Fiber), and MS (Motorized Stage) in the photo and schematic. This figure is reproduced from Hacker et al. [39]. Please click here to download this File.

Discussion

Here, a protocol is presented that aims to provide a versatile recipe for a stable, biologically relevant material that can be used to create phantoms for calibration measurements and standardization across multimodal acoustic and optical

Copyright © 2023 JoVE Creative Commons Attribution 3.0 License

biomedical imaging applications. The material has previously been shown to be stable over time[39], to have high batch-to-batch reproducibility, to be safe to use, and to consist of readily available, cost-effective ingredients from standard scientific suppliers. The material properties are independently tunable across relevant acoustic and optical regimes. Furthermore, it is mechanically robust and insoluble in water, thereby withstanding rough handling, and it is inert to water-based coupling agents that are used in ultrasonic/photoacoustic research. It was highlighted that different phantom designs can be created with different types of inclusions, composed of the same or of different material types. Given these properties, the material fulfills the aforementioned key criteria for an ideal biophotonic phantom and shows key advantages compared to other existing tissue-mimicking materials[3]. By detailing the exact manufacturing process, we hope to minimize variations arising from the fabrication procedure, thereby optimizing its use for calibrating, validating, and tracking the performance of imaging systems.

Two key steps have been identified as being critical to the fabrication process. First, ingredients need to be thoroughly mixed and uniformly heated for the creation of a homogenous material. Using a sonicator and magnetic stirrer for mixing and an oil bath for heating ensures the even distribution of material components within the base matrix. Care needs to be taken that the oil bath does not reach very high temperatures (>180 °C), as this will result in oxidation of the material components, leading to yellowish discoloration. Manual stirring can support the mixing process and compensates for insufficient heating from the material-air interface. The time for sonication and mixing may need to be extended when a higher concentration of TiO_2 and/or polymers are used to ensure a homogenous composition of the material. Second, air bubbles need to be removed to prevent the formation of heterogeneities within the base matrix. Whilst this can be achieved with a vacuum pump or oven, careful pouring from a low height should also be practiced to minimize trapping air within the material.

One significant advantage of the material is its thermoplastic properties (derived from the SEBS polymer), allowing it to be reheated and remolded without any significant impact on its acoustic and optical properties[39]. However, reheating needs to be performed gradually and carefully, as the material can easily burn and oxidize if reheated too quickly. Reheating also becomes more difficult when higher LDPE concentrations are used, as LDPE does not exhibit the same thermoplastic behavior as SEBS.

Several limitations of the protocol remain. Due to the high melting temperature of the polymers (150 °C), phantom molds need to made out of a heat-resistant material, such as glass or stainless steel. Additionally, the material is fairly viscous in liquid state if a high polymer concentration is used to tune the acoustic properties, making the filling of small imaging targets difficult. Finally, tuning of the acoustic properties is thus far limited to a speed of sound range of ~1450-1,516 $m \cdot s^{-1}$ which supports mimicking tissues such as breast or fat (c = 1,450-1,480 $m \cdot s^{-1}$), but may be insufficient for tissues like muscle or kidney (c > 1,520 $m \cdot s^{-1}$). The concomitant change of acoustic attenuation should also be taken into consideration.

Here, we have highlighted the application of the material as a stable phantom for ultrasound and optical imaging applications. However, copolymer-in-oil materials have also shown to be of value in elastography applications[35], and could potentially allow for compatibility with further imaging modalities such as magnetic resonance imaging. Increased anatomical realism of the phantoms may be achieved using

Copyright © 2023 JoVE Creative Commons Attribution 3.0 License

3D-printed molds, as shown in similar studies[29,47,48,49]. Early studies have also demonstrated the 3D printability of the material itself, further extending its flexibility in terms of processing and fabrication. These developments highlight the exciting future potential of the material as a widely used, stable phantom medium for multimodal imaging applications.

Disclosures

Sarah Bohndiek has previously received research support from CYBERDYNE INC and iThera Medical GmbH, vendors of photoacoustic imaging instruments. The other authors have no conflict of interest related to the present manuscript to disclose.

Acknowledgments

LH was funded by NPL's MedAccel program financed by the Department for Business, Energy and Industrial Strategy's Industrial Strategy Challenge Fund. JMG received funding from the Deutsche Forschungsgemeinschaft (DFG, German Research Foundation) under project GR 5824/1. JJ acknowledges the funding support from Academy of Medical Sciences Springboard (REF: SBF007\100007) award. SEB acknowledges support from Cancer Research UK under grant number C9545/A29580. AMI, BZ, and SR were supported by U.K. Department for Business, Energy & Industrial Strategy via funding of the National Measurement System. **Figure 1** and **Figure 2** were created with BioRender.

References

1. Waterhouse, D. Translation of optical imaging biomarkers: opportunities and challenges. *Nature Biomedical Engineering.* **3** (5), 339-353 (2019).
2. O'Connor, J. P. B. et al. Imaging biomarker roadmap for cancer studies. *Nature Reviews Clinical Oncology.* **14** (3), 169-186 (2017).
3. Hacker, L. et al. Criteria for the design of tissue-mimicking phantoms for the standardization of biophotonic instrumentation. *Nature Biomedical Engineering.* **6** (5), 541-558 (2022).
4. Laufer, J., Zhang, E., Beard, P. Evaluation of absorbing chromophores used in tissue phantoms for quantitative photoacoustic spectroscopy and imaging. *IEEE Journal of Selected Topics in Quantum Electronics.* **16** (3), 600-607 (2010).
5. Cook, J. R., Bouchard, R. R., Emelianov, S. Y. Tissue-mimicking phantoms for photoacoustic and ultrasonic imaging. *Biomedical Optics Express.* **2** (11), 3193-3206 (2011).
6. Xia, W. et al. Poly(vinyl alcohol) gels as photoacoustic breast phantoms revisited. *Journal of Biomedical Optics.* **16** (7), 075002 (2011).
7. Manohar, S. et al. Photoacoustic mammography laboratory prototype: imaging of breast tissue phantoms. *J Biomed Opt.* 9, 1172 (2004).
8. Blumenröther, E., Melchert, O., Wollweber, M., Roth, B. Detection, numerical simulation and approximate inversion of optoacoustic signals generated in multi-layered PVA hydrogel based tissue phantoms. *Photoacoustics.* **4** (4), 125-132 (2016).
9. Kharine, A. et al. Poly(vinyl alcohol) gels for use as tissue phantoms in photoacoustic mammography. *Physics in Medicine and Biology.* **48** (3), 357-370 (2003).
10. Spirou, G. M., Oraevsky, A. A., Vitkin, I. A., Whelan, W. M. Optical and acoustic properties at 1064 nm of

Copyright © 2023 JoVE Creative Commons Attribution 3.0 License

polyvinyl chloride-plastisol for use as a tissue phantom in biomedical optoacoustics. *Physics in Medicine and Biology.* **50** (14), N141-N153 (2005).

11. Bohndiek, S. E., Bodapati, S., Van De Sompel, D., Kothapalli, S.-R., Gambhir, S. S. Development and application of stable phantoms for the evaluation of photoacoustic imaging instruments. *PLoS One.* **8** (9), e75533 (2013).
12. Fonseca, M., Zeqiri, B., Beard, P. C., Cox, B. T. Characterisation of a phantom for multiwavelength quantitative photoacoustic imaging. *Physics in Medicine and Biology.* **61** (13), 4950-4973 (2016).
13. Vogt, W. C., Jia, C., Wear, K. A., Garra, B. S., Joshua Pfefer, T. Biologically relevant photoacoustic imaging phantoms with tunable optical and acoustic properties. *Journal of Biomedical Optics.* **21** (10), 101405 (2016).
14. Dantuma, M., van Dommelen, R., Manohar, S. Semi-anthropomorphic photoacoustic breast phantom. *Biomedical Optics Express.* **10** (11), 5921-5939 (2019).
15. Jeong, E. et al. Fabrication and characterization of PVCP human breast tissue-mimicking phantom for photoacoustic imaging. *BioChip Journal.* **11**, 67-75 (2017).
16. Jia, C., Vogt, W. C., Wear, K. A., Pfefer, T. J., Garra, B. S. Two-layer heterogeneous breast phantom for photoacoustic imaging. *Journal of Biomedical Optics.* **22** (10), 1-14 (2017).
17. Madsen, E. L., Hobson, M. A., Shi, H., Varghese, T., Frank, G. R. Stability of heterogeneous elastography phantoms made from oil dispersions in aqueous gels. *Ultrasound in Medicine & Biology.* **32** (2), 261-270 (2006).
18. Culjat, M. O., Goldenberg, D., Tewari, P., Singh, R. S. A review of tissue substitutes for ultrasound imaging. *Ultrasound in Medicine & Biology.* **36** (6), 861-873 (2010).
19. Zell, K., Sperl, J. I., Vogel, M. W., Niessner, R., Haisch, C. Acoustical properties of selected tissue phantom materials for ultrasound imaging. *Physics in Medicine and Biology.* **52** (20), N475-N484 (2007).
20. Lazebnik, M., Madsen, E. L., Frank, G. R., Hagness, S. C. Tissue-mimicking phantom materials for narrowband and ultrawideband microwave applications. *Physics in Medicine and Biology.* **50** (18), 4245-4258 (2005).
21. Ramnarine, K. V., Anderson, T., Hoskins, P. R. Construction and geometric stability of physiological flow rate wall-less stenosis phantoms. *Ultrasound in Medicine & Biology.* **27** (2), 245-250 (2001).
22. Pogue, B. W., Patterson, M. S. Review of tissue simulating phantoms for optical spectroscopy, imaging and dosimetry. *Journal of Biomedical Optics.* **11** (4), 041102 (2006).
23. Lamouche, G. et al. Review of tissue simulating phantoms with controllable optical, mechanical and structural properties for use in optical coherence tomography. *Biomedical Optics Express.* **3** (6), 1381-1398 (2012).
24. Bohndiek, S. E., Van de Sompel, D., Bodapati, S., Kothapalli, S. R., Gambhir, S. S. Stable phantoms for characterization of photoacoustic tomography (PAT) systems. In *Design and Performance Validation of Phantoms Used in Conjunction with Optical Measurement of Tissue V.* **858308**, 30-35 (2013).

Copyright © 2023 JoVE Creative Commons Attribution 3.0 License

25. Fenollar, O., Sanchez-Nacher, L., Garcia-Sanoguera, D., López, J., Balart, R. The effect of the curing time and temperature on final properties of flexible PVC with an epoxidized fatty acid ester as natural-based plasticizer. *Journal of Materials Science.* **44**, 3702-3711 (2009).
26. Fonseca, M., Zeqiri, B., Beard, P., Cox, B. Characterisation of a PVCP-based tissue-mimicking phantom for quantitative photoacoustic imaging. In *European Conference on Biomedical Optics.* Optica Publishing Group. 953911 (2015).
27. Heudorf, U., Mersch-Sundermann, V., Angerer, J. Phthalates: toxicology and exposure. *International Journal of Hygiene and Environmental Health.* **210** (5), 623-634 (2007).
28. Maneas, E. et al. Gel wax-based tissue-mimicking phantoms for multispectral photoacoustic imaging. *Biomed. Opt. Express.* **9** (3), 1151-1163 (2018).
29. Maneas, E. et al. Anatomically realistic ultrasound phantoms using gel wax with 3D printed molds. *Physics in Medicine and Biology.* **63** (1), 015033 (2018).
30. Jones, C. J. M., Munro, P. R. T. Stability of gel wax based optical scattering phantoms. *Biomedical Optics Express.* **9** (8), 3495-3502 (2018).
31. Ivory, A. M., Shah, A., Rajagopal, S., Zeqiri, B. Development and investigation of the acoustic properties of tissue-mimicking materials for photoacoustic imaging techniques. in *IEEE International Ultrasonics Symposium.* IEEE. 1489-1492 (2019).
32. Grillo, F. W., Cabrelli, L. C., Sampaio, D. R. T., Carneiro, A. A. O., Pavan, T. Z. Glycerol in oil-based phantom with improved performance for photoacoustic imaging. In *2017 IEEE International Ultrasonics Symposium.* IEEE. 1-4 (2017).
33. Cabrelli, L. C. et al. Oil-based gel phantom for ultrasound and optical imaging. In *Biophotonics South America.* SPIE. **9531**, 40-46 (2015).
34. Cabrelli, L. C. et al. Stable phantom materials for ultrasound and optical imaging. *Physics in Medicine and Biology.* **62** (2), 432-447 (2017).
35. Oudry, J., Bastard, C., Miette, V., Willinger, R., Sandrin, L. Copolymer-in-oil phantom materials for elastography. *Ultrasound in Medicine & Biology.* **35** (7), 1185-1197 (2009).
36. Suzuki, A. et al. Oil gel-based phantom for evaluating quantitative accuracy of speed of sound measured in ultrasound computed tomography. *Ultrasound in Medicine & Biology.* **45** (9), 2554-2567 (2019).
37. Cabrelli, L. C., Grillo, F. W., Carneiro, A. A. O., Pavan, T. Z. Copolymer-in-oil tissue-mimicking material with tunable acoustic properties. in *2016 IEEE International Ultrasonics Symposium.* IEEE. 1-4 (2016).
38. Cabrelli, L. C. et al. Copolymer-in-oil phantoms for photoacoustic imaging. in *2015 IEEE International Ultrasonics Symposium.* IEEE. 1-4 (2015).
39. Hacker, L. et al. A copolymer-in-oil tissue-mimicking material with tuneable acoustic and optical characteristics for photoacoustic imaging phantoms. *IEEE Transactions on Medical Imaging.* **40** (12), 3593-3603 (2021).
40. Greenspan, M., Tschiegg, C. E. Speed of sound in water by a direct method. *Journal of Research of the National Bureau of Standards.* **59** (4), 249-254 (1957).

Copyright © 2023 JoVE Creative Commons Attribution 3.0 License

41. Zeqiri, B., Scholl, W., Robinson, S. P. Measurement and testing of the acoustic properties of materials: a review. *Metrologia.* **47** (2), S156-S171 (2010).

42. Pickering, J. W. et al. Double-integrating-sphere system for measuring the optical properties of tissue. *Applied Optics.* **32** (4), 399-410 (1993).

43. Rajagopal, S., Sadhoo, N., Zeqiri, B. Reference characterisation of sound speed and attenuation of the IEC agar-based tissue-mimicking material up to a frequency of 60 MHz. *Ultrasound in Medicine & Biology.* **41** (1), 317-333 (2015).

44. Prahl, S. A. *Everything I think you should know about Inverse Adding-Doubling. Oregon Medical Laser Center, St. Vincent Hospital.* **1344**, 1-74 (2011).

45. Pinkerton, J. M. M. The absorption of ultrasonic waves in liquids and its relation to molecular constitution. *Proceedings of the Physical Society. Section B.* **62** (2), 129-141 (1949).

46. Hu, D., Lu, R., Huang, Y., Ying, Y., Fu, X. Effects of optical variables in a single integrating sphere system on estimation of scattering properties of turbid media. *Biosystems Engineering.* **194**, 82-98 (2020).

47. Grillo, F. W. et al. Patient-specific neurosurgical phantom: assessment of visual quality, accuracy, and scaling effects. *3D Printing in Medicine.* **4** (1), 3 (2018).

48. Nikitichev, D. I. et al. Construction of 3-dimensional printed ultrasound phantoms with wall-less vessels. *Journal of Ultrasound in Medicine.* **35** (6), 1333-1339 (2016).

49. West, S. J. et al. Development of an ultrasound phantom for spinal injections with 3-dimensional printing. *Regional Anesthesia and Pain Medicine.* **39** (5), 429-433 (2014).

Copyright © 2023 JoVE Creative Commons Attribution 3.0 License